Eur. Phys. J. B **30**, 57–66 (2002)
DOI: 10.1140/epjb/e2002-00358-7

THE EUROPEAN PHYSICAL JOURNAL B

Electronic topological transitions and phase stability in the fcc Al-Zn alloys

E.A. Smirnova[1], P.A. Korzhavyi[2,a], Yu. Kh. Vekilov[1], B. Johansson[2,3], and I.A. Abrikosov[3]

[1] Department of Theoretical Physics, Moscow State Institute of Steel and Alloys, 119991 Moscow, Russia
[2] Department of Materials Science and Engineering, Royal Institute of Technology, 10044 Stockholm, Sweden
[3] Condensed Matter Theory Group, Department of Physics, Uppsala University, 75121 Uppsala, Sweden

Received 6 February 2002
Published online 19 November 2002 –

Abstract. We report on a detailed investigation of the phase equilibria and the Fermi surface in the Al-Zn system. Our calculation are based on the density functional theory and we use the linear muffin-tin orbital method and the Green's function technique. The calculated free energies of alloy formation exhibit the existence of a miscibility gap between the alloys containing approximately 10 and 55 at.% of Zn, in agreement with the phase diagram of the Al-Zn system. Seven electronic topological transitions (ETT) were found in Al-Zn system within the stability range of the fcc solid solution. A relation between these ETT and the phase stability of the fcc Al-Zn solid solutions is established. We show that extremum points on the concentration dependencies of the thermodynamic properties of Al-Zn alloys can be explained by band-filling effects.

PACS. 71.23.-k Electronic structure of disordered solids – 71.18.+y Fermi surface: calculations and measurements

1 Introduction

It is well-known that from the microscopic point of view there must exist a connection between the peculiarities of electronic spectrum of an alloy and the phase stability in the system [1–7]. For example, the changes in the band filling caused by the alloying between two elements may lead to changes in the Fermi surface topology, and thus lead to the peculiarities of the alloy properties. It has been shown theoretically [8] and experimentally [9] that these so-called electronic topological transitions (ETT) affect certain kinetic and thermodynamic properties of metals and alloys such as thermopower, residual resistivity, the coefficient of thermal expansion, elastic moduli, etc. in the vicinity of the transition point [10–15]. In the present work we perform a detailed investigation of relations between the ETT and the the alloy phase stability by studying the electronic nature of the isostructural spinodal decomposition in the Al-Zn system. Recently we have shown that the ETT do exist in the Al-Zn system, and that these transitions influence the phase equilibria in the Al-Zn system and they account for an assymetry of the miscibility gap on the phase diagram [16]. In the present paper we report in detail on the results of our investigation.

A phase diagram of the Al-Zn binary system is shown in Figure 1a. There are no stable ordered intermetallic

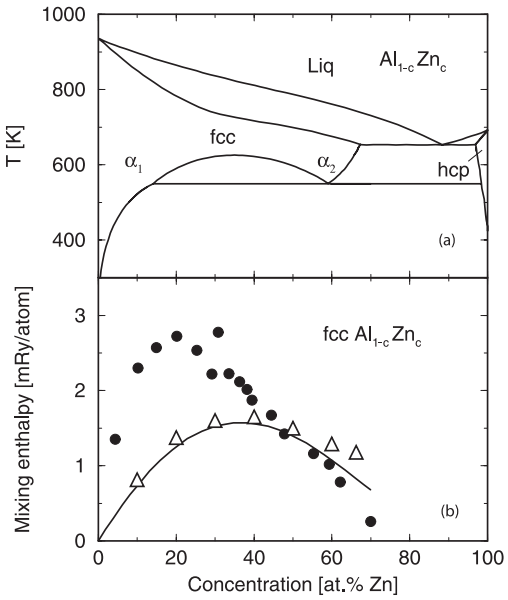

Fig. 1. (a) Experimental Al-Zn phase diagram, redrawn from reference [17]; (b) Experimental energy of mixing of the fcc Al-Zn random alloys compiled from different sources. Data presented in reference [17] (triangles) and reference [18] (circles) are recalculated to account for the fcc-hcp structural energy difference of Zn, see text. Solid line in (b) shows the CALPHAD estimation of the enthalpy of mixing presented in reference [19].

[a] e-mail: pavel@met.kth.se

compounds in this system. A random substitutional fcc solid solution of Zn in Al is stable up to 66.5 at.% Zn at high temperatures. At temperatures below 624.6 K, a miscibility gap opens up between two (α_1 and α_2) fcc solid solutions. However, the monotectoid line has its maximum at 39.5 at.% Zn, rather than at the equiatomic composition, as one could expect in the model of regular solid solutions. The concentration of the spinodal point, in fact, coincides with a maximum of the measured mixing energy in this system (Fig. 1b) [17–19]. At temperatures below 548 K, the α_2 solid solution with the concentration of 59.4 at.% Zn becomes unstable, the solubility of Zn in the α_1 phase rapidly decreases with decreasing the temperature, and a wide two-phase region exists between α_1 fcc solid solution and a Zn-based solid solution. Due to this feature, Al-Zn alloys have attracted great attention as a model alloy system for studies of spinodal [20] and discontinuous [21] decomposition, as well as of second phase precipitation [22,23].

The existence of a miscibility gap between two fcc solid solutions which differ only in their concentrations is very interesting from the theoretical point of view. The atomic radii of Al (1.43 Å) and Zn (1.37 Å) are very close to each other, so are their electronegativities (1.61 and 1.65, respectively), and even their bulk moduli are quite similar (72.2 GPa and 59.8 GPa). The two major differences are their equilibrium crystal structures (fcc for Al and hexagonal for Zn), and the electron-per-atom ratio (roughly speaking, an Al atom has three valence electrons, whereas a Zn atom has only two). The role of the crystal structure contribution to the solid solubility in metallic alloys is well-known [24], and for the Al-Zn system it was recently elucidated by Müller *et al.* [22]. But, as a matter of fact, crystal structure itself is determined by the electronic structure factor [25,26]. In particular, taking into account the complexity of the Fermi surface of pure Al, one can expect that the changes in the band filling caused by the addition of Zn to Al may lead to ETTs and, therefore, influence the phase stability in this system.

2 Alloy stability upon the electronic topological transition

Alloy stability against a spinodal decomposition (or, equivalently, against infinitesimal fluctuations of the alloy concentration apart from its average value c) is determined by the second derivative of the free energy $\mathrm{d}^2F/\mathrm{d}c^2$. A negative value of the second derivative means absolute instability, whereas a positive value means that the alloy is metastable, *i.e.* that a certain nucleation energy is required to begin the process of alloy decomposition [4]. At the same time, one of the main contributions to the alloy formation energy, and thus to its second derivative, comes from the one-electron energy (band structure) term. Moreover, the second derivative of the alloy formation energy is governed by the electron density of states at the Fermi level. Qualitatively, this conclusion can be derived within the simplest rigid-band model which is formulated below.

Let us consider a binary alloy $A_{1-c}B_c$ and assume that its components form a common rigid *sp*-band. In this case the only change of the electronic structure upon variation of concentration would be a change of the band filling. Let us denote the valence numbers of alloy components A and B as N_A and N_B, respectively, and their difference as $\Delta = N_B - N_A$. Then one can calculate the one-electron energy contribution to the total energy of the alloy, because this is the only term that explicitly depends on the DOS, $n(\varepsilon)$:

$$E_{bs} = \int_{\varepsilon_b}^{\varepsilon_F} \varepsilon\ n(\varepsilon)\mathrm{d}\varepsilon, \tag{1}$$

where ε_b is the valence band bottom. The Fermi level, ε_F, is determined by the mean number of valence electrons per atom,

$$\bar{N} = \int_{\varepsilon_b}^{\varepsilon_F} n(\varepsilon)\ \mathrm{d}\varepsilon, \tag{2}$$

or, correspondingly, by the alloy concentration $c = (\bar{N} - N_A)/\Delta$.

The band-structure contribution to the second derivative of the alloy formation energy is then

$$\frac{\mathrm{d}^2E_{bs}}{\mathrm{d}c^2} = \frac{\Delta^2}{n(\varepsilon_F)}\cdot \tag{3}$$

According to the one-electron theory of electronic topological transitions in alloys [8,10,13], the alloy properties which are high-order derivatives of the thermodynamic potential with respect to the parameter of proximity to the transition point must become singular at the ETT [28]. For instance, the second derivative of the thermodynamic potential is expected to have singularities of the same type as the singularities in the density of electron states. In the ideal case of an ETT at zero temperature and without a smearing due to disorder, the density of states near the transition point consists of two parts, a regular part n^{reg} and a singular part n^{sing},

$$n(\varepsilon) = n^{reg}(\varepsilon) + n^{sing}(\varepsilon) = n_0 + \begin{cases} \alpha(\varepsilon - \varepsilon^*)^{1/2},\ \varepsilon > \varepsilon^* \\ 0,\ \varepsilon < \varepsilon^* \end{cases} \tag{4}$$

where ε^* is the critical point. Thus, the DOS shows a square root-type singularity when the ETT occurs.

In general, this peculiarity is quite weak [15,29]. However, as has been pointed out by Katsnelson *et al.* [30], a stronger singularity $n^{sing}(\varepsilon) \sim ln|\varepsilon - \varepsilon^*|$ may occur as a result of confluence of two square root-type singularities. As a result, see equation (3), one can expect superior stability of an alloy whose Fermi level falls into a minimum of the DOS in a vicinity of such a ETT, and *vice versa* for the maximum. The discussion above establishes a connection between the ETT and the alloy stability with respect to the spinodal decomposition.

3 Computational technique

3.1 Details of calculations

Our electronic structure calculations were based on the density functional theory [31,32] and made use of the local density approximation (LDA) for the one-electron potential including the non-local corrections in the framework of the generalized gradient approximation (GGA) [33]. We employ a basis set of the linear muffin-tin orbitals (LMTO) of Andersen and co-workers [34–39]. Since the $3d$ states of Zn are fully occupied and are located close to the bottom of the valence band, we had to consider both the $3d$ and $4d$ states of Zn as valence states. In order to have a good description of the wave functions and electron density on the Zn site, we calculated the exact energy dependence of the potential function rather than used its LMTO parametrization. The core states of Al and Zn were recalculated at each loop of the self-consistency procedure. The atomic spheres of the alloy components were taken to be equal to the average Wigner-Seitz radius in the alloy.

Brillouin zone integration was done with the help of the special point technique, [40] covering 2304 special **k**-points in the 1/48 irreducible wedge of the Brillouin zone for the fcc lattice. The density of states (DOS) moments were evaluated by integration along a complex energy contour on which 20 energy points were distributed in a logarithmic (Gaussian) mesh. The equilibrium lattice parameter and the corresponding ground state properties of each alloy were obtained on the basis of 6 self-consistent calculations at different lattice parameters close to the total energy minimum. The equation of state for each alloy was obtained by fitting the calculated total energies using the 4th order polynomials.

3.2 Treatment of disorder

We considered random Al-Zn alloys using two different approaches within alloy theory, the coherent potential approximation (CPA) [41–44] and the locally self-consistent Green's function (LSGF) method [45,46]. Within these methods it is assumed that there exists an underlying crystal lattice, and the sites of this lattice are occupied by the alloy components with certain probabilities. The size mismatch of the alloy components in the Al-Zn alloy is quite small. Although lattice distortions are certainly essential for certain problems such as, for example, the problem of calculating the equilibrium shape of precipitates in this system [23], their effect on the total energy is minute and fairly symmetric relative to the equiatomic composition [22]. Thus, for our discussion the local distortions of the underlying lattice can be safely neglected.

Within the CPA the occupation of each site of the underlying lattice does not depend on the occupation of neighboring sites, *i.e.* the short-range order effects are also neglected. The average one-electron Green's function is calculated for an ordered lattice of effective scatterers that replaces the real disordered alloy. The properties of these effective atoms are determined self-consistently within the single-site approximation under the condition that the scattering of electrons off real atoms embedded in the effective medium vanishes on the average. The CPA is probably the most efficient approximation that allows one to calculate such alloy properties as the electronic structure and the Fermi surface [14,15,27,43,47–51]. Its accuracy has recently been reexamined by several authors [52–54], and the conclusion is that the CPA densities of states and total energies for a completely random alloy agree well with those calculated by methods which go beyond the single-site approximation, like the LSGF method also used in the present work.

The LSGF method is a linear (order-N) scaling method of electronic structure calculations for large supercells with an arbitrary distribution of atoms of different kinds on an underlying crystal lattice. The order-N scaling is achieved by associating each atom in the system with its so-called local interaction zone (LIZ) [55,56]. Inside each LIZ the multiple scattering problem, formulated in terms of the Dyson equation for the LIZ Green's function, is solved exactly. The convergence of the method is controlled by the size of the LIZ, and its minimal size is ensured by embedding the LIZ into a self-consistent effective medium. In contrast to the CPA, the LSGF method allows one to include short-range order effects in alloys [45,57]. Also, it solves one of the problems arising in *ab initio* implementations of the CPA, namely, it allows one to calculate the electrostatic contribution to the one-electron potential and energy of an alloy exactly within the shape approximation which is used for the one-electron potential and charge density. Usually, a spherical approximation is used, either the muffin-tin (MT) or the atomic sphere approximation (ASA). Moreover, within the LSGF one can improve on accuracy of calculations by going beyond the ASA for the charge density but keeping the ASA for the potential. This so-called ASA+M approach turns out to have sufficient accuracy for surface energy [58] and vacancy formation energy [59] calculations. As will be presented elsewhere, it is essential to include these multipole corrections in order to obtain accurate total energies of Al-Zn alloys, as it is probably the general case for random alloys between the *sp*-metals.

Thus, on one hand, we face a problem of calculating the Fermi surface, and also of performing total energy calculations on a very fine grid of concentrations in order to calculate the derivatives, equation (3), where one would prefer to apply the CPA. On the other hand, we need a description of the electrostatic contribution to the one-electron potential and energy, including multipole corrections, with an accuracy of at least the LSGF ASA+M calculations. In the next section we will show that a compromise can be found within the modified screened impurity model (SIM).

3.3 Screened impurity model

The screened impurity model developed in references [14,60–62] is a simple model for estimating the

electrostatic contribution to the one-electron potentials of atoms in a random alloy, and to the alloy total energy. This contribution exists due to a nonzero value of the net charge on an alloy component i,

$$Q_i = \int_{S_{WS}} \mathrm{d}^3 r \rho_i - Z_i, \tag{5}$$

where S_{WS}, Z_i and ρ_i are the Wigner-Seitz radius, the atomic number and the electron density of component i, respectively. The SIM is based on two simple assumptions, that this net charge *on the average* is completely screened by the first shell of effective atoms, and that the screening charge is uniformly distributed among these atoms. Recently, these assumptions have been justified by Ruban and Skriver by means of the supercell LSGF calculations [64].

Note, that in earlier studies of this problem [14,60–64] only the monopole contributions to the one-electron potential and energy were taken into consideration. As have been mentioned above, the multipole contributions may also be important in alloys of simple metals. Here we modify the SIM in the spirit of reference [64] and calculate the electrostatic contributions to the one-electron potential of alloy components, as well as to the total energy of a binary alloy, using the following expressions:

$$\begin{aligned} V_M^i &= -e^2 \frac{Q_i}{R_{\mathrm{eff}}} \\ E_M &= -\frac{1}{2}\beta e^2 c(1-c)\frac{(Q_A - Q_B)^2}{R_{\mathrm{eff}}}, \end{aligned} \tag{6}$$

where e is the electron charge and the screening radius R_{eff}, as well as the prefactor β, are two parameters of the model. We remark, that within the ASA the R_{eff} is usually found to be close to the radius of the first coordination shell, R_1, and a value of $\beta \approx 1.2$ brings the total energy of a random alloy in the framework of the CPA in agreement with the total energy calculated within the LSGF [53,64]. Below we will show that β and R_{eff} can be chosen in such a way that the CPA calculations reproduce the results of the LSGF calculations within the *ASA+M* method.

In our LSGF ASA+M calculations [59], the random Al-Zn alloys having the atomic fraction of Zn equal to 1/8, 1/6, 1/4, 1/3, 3/8, 1/2, 2/3, and 5/6 were modeled by supercells with a quasirandom distribution of atoms (with zero Warren-Cowley short-range order parameters up to the 4th coordination shell). The number of terms included in the multipole expansions of the Madelung potential and energy is determined by the angular momentum cutoff l_{max} used in the Green's functions calculations. In the present calculations we used $l_{max} = 3$ and considered all the nonzero multipole moments of the charge density up to $l = 2l_{max} = 6$.

From the results of the LSGF ASA+M calculations we determined the following SIM parameters: the effective screening radius, $R_{\mathrm{eff}} = 0.731R_1$, and the Madelung energy prefactor, $\beta = 1.144$. The CPA calculations were then performed for the random Al-Zn alloys in the whole concentration interval. In Figure 2 the difference of the net charges inside the Al and Zn atomic spheres, $\Delta Q = |Q_{Al} - Q_{Zn}|$, calculated using the LSGF ASA+M method and the CPA method, is plotted as a function of concentration. One can see that charges inside the AS agree very well with each other. For comparison, we also show the results of the LSGF ASA (*i.e.* without multipole contributions) and the CPA SIM calculations with a conventional parameter $R_{\mathrm{eff}} = R_1$. Note that the LSGF ASA and the CPA SIM ($R_{\mathrm{eff}} = R_1$) results agree satisfactorily with each other, but both sets of results are quite different from those calculated within the LSGF ASA+M and CPA SIM ($R_{\mathrm{eff}} = 0.731R_1$) schemes.

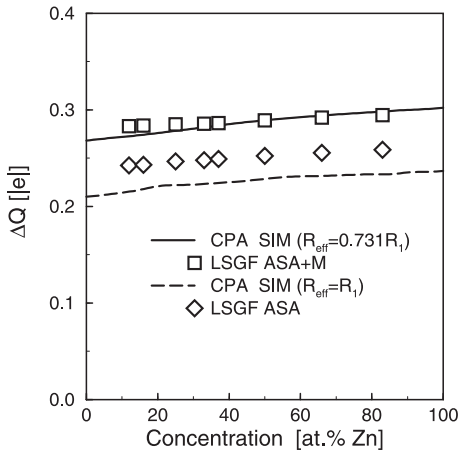

Fig. 2. Difference of the net charges inside the Al and Zn atomic spheres, $\Delta Q = |Q_{\mathrm{Al}} - Q_{\mathrm{Zn}}|$, calculated using the LSGF method with the multipole corrections included by means of ASA+M technique (squares) and the CPA SIM ($R_{\mathrm{eff}} = 0.731R_1$) scheme (full line). Also shown for comparison the ΔQ calculated within the LSGF-ASA method (diamonds) and within the conventional CPA SIM ($R_{\mathrm{eff}} = R_1$) scheme (dashed line).

Table 1. Mixing energies E_{mix} [mRy/atom] and lattice parameters [Å] of random fcc Al-Zn alloys, obtained by means of the LSGF ASA+M and CPA SIM ($R_{\mathrm{eff}} = 0.731R_1$) calculations.

c_{Zn}	E_{mix}		Lattice parameter	
	CPA	LSGF	CPA	LSGF
12.5	0.74	0.75	3.968	3.968
16.7	0.90	0.88	3.965	3.965
25.0	1.05	0.98	3.959	3.958
33.3	1.01	0.95	3.951	3.951
37.5	0.93	0.88	3.947	3.947
50.0	0.60	0.60	3.935	3.935
66.7	0.30	0.35	3.922	3.920
83.3	0.17	0.19	3.909	3.906

In Table 1 we summarize the most important ground state properties, the mixing energies E_{mix} and the lattice parameters of Al-Zn alloys, obtained by means of the LSGF ASA+M and CPA SIM calculations. Again, one can see very good agreement between them in the whole

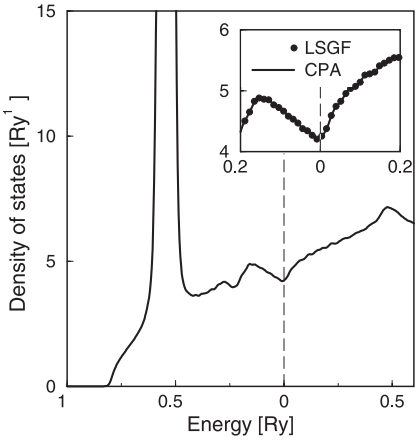

Fig. 3. Density of states of the fcc $Al_{50}Zn_{50}$ random alloy as a function of energy (relative to the Fermi energy) calculated using the LSGF ASA+M and the CPA SIM ($R_{\rm eff} = 0.731R_1$) methods. Results are indistinguishable from each other. Insert shows an energy window around the Fermi level where the CPA SIM curve is drawn by the full line, while the LSGF ASA+M data are given by circles.

compositional range of stability of fcc Al-Zn alloys. In Figure 3 the densities of states for the $Al_{50}Zn_{50}$ random alloy, obtained by the two above mentioned techniques, are presented. The LSGF ASA+M and the CPA SIM densities of states are almost indistinguishable from each other. The inset in Figure 3 shows, for a small energy window around the Fermi level, that the CPA DOS (dots) follows exactly the DOS calculated using the LSGF ASA+M (solid line). Therefore, we conclude that the electronic structure and cohesive properties of random fcc Al-Zn alloys can be adequately represented by the CPA SIM scheme.

4 Results and discussion

4.1 Fermi surface topology in Al-Zn alloys

The Fermi surfaces of the alloys were depicted using the results of the Bloch spectral density (BSD) $A(\mathbf{k}, E_F)$ calculations [65] for the (001) section of the Brillouin zone. The Fermi surface was associated with the **k**-space positions of the BSD peaks at Fermi energy E_F. These peaks were found to be rather sharp even for concentrated alloys. This means that the Fermi electron lifetime is rather long, and the Fermi surfaces in Al-Zn alloys are well-defined. In more details the technique used in the present study was outlined in reference [15].

In Figure 4a we show the Fermi surface of pure fcc Al, and in Figure 5 the band structure of Al is given in order to emphasize its connection with the Fermi surface. One can see that the first band is fully occupied (the whole band is below the Fermi level). The second and the third bands are partially filled. The lenses at the faces of the Brillouin zone correspond to occupied electron states of the second band, whereas the feature near point K(U) and the small pockets on line W-X correspond to electron states of the

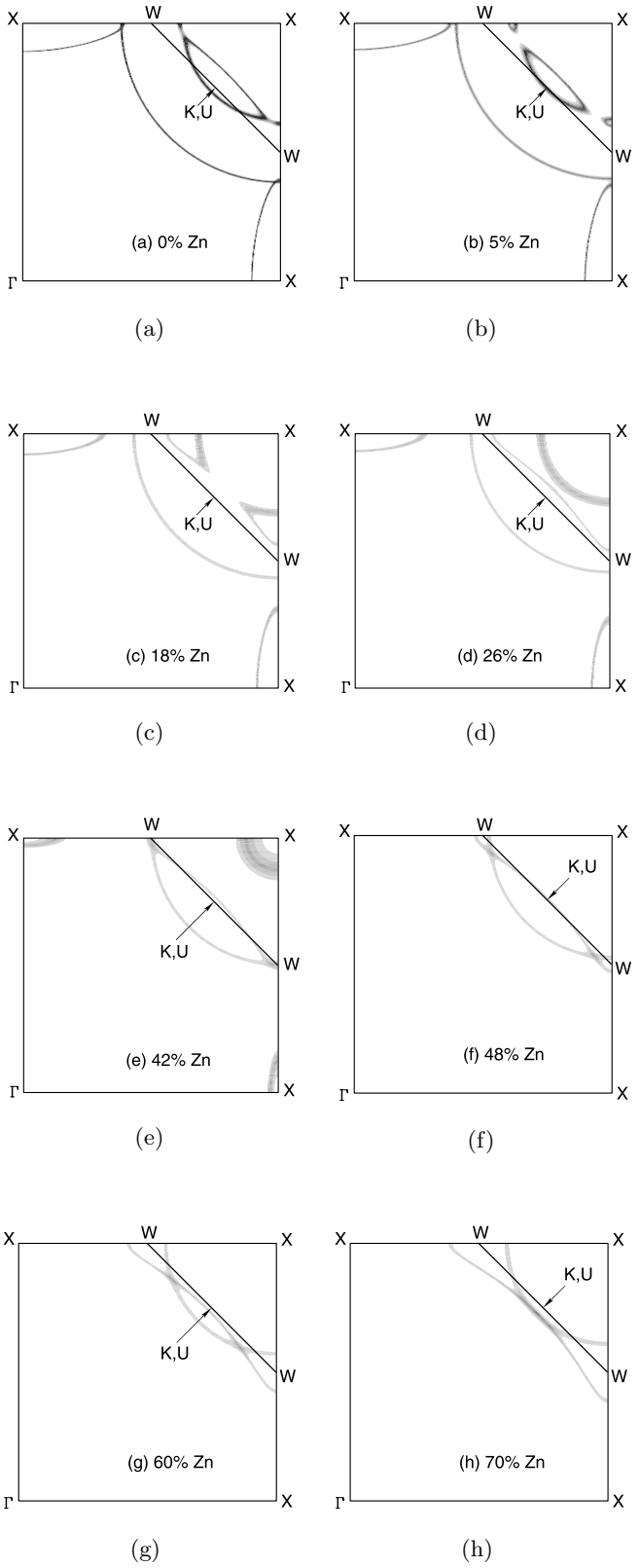

Fig. 4. Sections of the Fermi surface of fcc Al-Zn random alloys in the (001) plane at different alloy compositions, (a) pure fcc Al, (b) $Al_{95}Zn_{05}$, (c) $Al_{82}Zn_{18}$, (d) $Al_{74}Zn_{26}$, (e) $Al_{58}Zn_{42}$, (f) $Al_{52}Zn_{48}$, (g) $Al_{40}Zn_{60}$, (h) $Al_{30}Zn_{70}$.

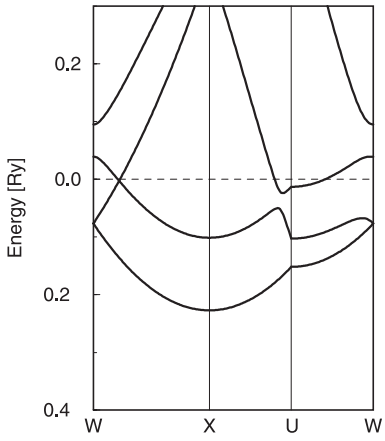

Fig. 5. Band structure of the fcc Al calculated within the ASA.

third band. We have found that 7 electronic topological transitions occur in Al-Zn alloys when the concentration of Zn increases from 0 to 70 at.%.

1-2. The first transition consists in the disappearance of the small electron pockets belonging to the third band on the line W-X ($0-3$ at.% Zn). The second topology change coincides with the first one. Due to the existence of a crossing point in the band structure of pure Al (Fig. 5), the disappearance of the electron regions on line W-X takes place simultaneously with a formation of a hole neck at the same k point on line W-X. This neck connects the large hole voids of the second band centered at Γ points of the adjacent Brillouin zones. Because of the symmetry, four such necks appear at each square face of the Brillouin zone. The two topological transitions described above can be seen when comparing Figures 4a and b.

3. Upon further addition of Zn, the electron region belonging to the third band on the square face becomes smaller, and disappears at a point on line U-X ($16-18$ at.% Zn), see Figures 4b and c. At the same time, the hole necks in the second band grow towards each other on the square face.

4. In Figure 4d we show that these necks have merged at a point on lines UX at $24-26$ at.% Zn. This also means that the second band electron region surrounding point X (center of a square face) becomes disconnected from the second band electron regions at hexagonal faces of the Brillouin zone.

5. A small hole pocket in the first band appears near point W ($40-42$ at.% Zn). Due to the disorder-induced smearing of the Fermi surface, the boundary of this pocket is almost illegible in Figure 4e, but it can be better seen in Figure 4f.

6. The electron regions of the second band on the square faces disappear at points X ($46-48$ at.% Zn), see Figure 4f.

Further increase of the Zn concentration leads to a narrowing of the necks between the second band electron regions centered on hexagonal faces, as can be seen in Figure 4g near point K.

7. At a concentration of Zn in the interval $68-70$ at.%, a neck forms to connect the hole pockets of the first band along the W-K-W line, Figure 4h.

The most important circumstance for the present system is that at two narrow concentration intervals several electronic topological transitions take place. Namely, transitions 1–3 occur at $3-16$ at.% Zn and transitions 5 and 6 occur at about $40-48$ at.% Zn. It is also important that the coinciding electronic topological transitions are of different kinds, *i.e.* they correspond to different topological changes of the Fermi surface. Therefore, in each of these two narrow concentration intervals, there are several *different* Van-Hove singularities in the density of electronic states. Although such singularities are smeared due to the substitutional disorder, especially in a concentrated alloy, they are still well-pronounced in the Al-Zn DOS because of the similarity of the scattering properties of Al and Zn.

4.2 Evolution of the alloy electronic structure and the ETT

Let us consider the densities of states of the disordered Al-Zn alloys. In the nearly-free-electron approximation the density of states for pure Al is square root-like. However, the crystal structure leads to a deformation of the energy bands at the boundaries of the Brillouin zone. As a result the density of states deviates from the nearly-free-electron behavior. For the pure Al, the Fermi level is situated on a slope of a peak (denoted by A in Fig. 6) of the density of states. Upon an increase of the Zn concentration both the number of occupied states in the alloy *sp*-band and the Fermi energy decrease. At first, this brings the Fermi level into a valley between peaks A and B (see Fig. 6), then pushes it up the peak B, and, finally, the Fermi level falls into a valley between peaks B and C at around 50 at.% of Zn. The evolution of the alloy DOS (Fig. 6) confirms this scenario. Indeed, at about 10 at. % of Zn the Fermi level passes through the DOS minimum between A and B peaks. This minimum can be associated with the almost complete disappearance of the third band states. The increase of the density of states at E_F with further increase of the Zn concentration is a result of the increase in the Fermi surface area associated with the growth of necks between the hole states regions of the second band. The DOS at the Fermi energy reaches maximum B (quite smeared due to disorder) with the disruption of the electron neck between the second band states, the fourth ETT, Figure 4d. Upon further increase of the Zn concentration the Fermi surface area of the second band electron states near point X decreases. Therefore, there is a decreasing contribution to the state density at the Fermi level. Complete disappearance of the second band electronic pocket near point X (Figs. 4e and f) coincides with the minimum of the DOS at the Fermi energy (a valley between peaks B and C, Fig. 6). Further addition of Zn leads to the increase of the density of states at the Fermi level due to the growth of the hole pockets corresponding to the first band around point W.

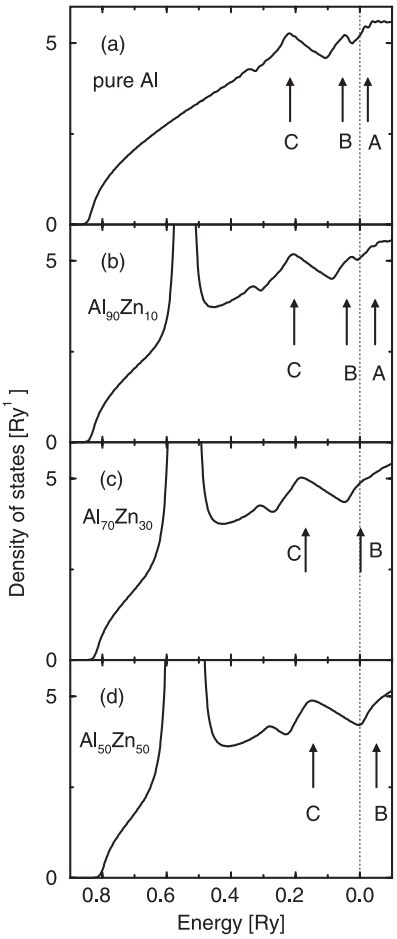

Fig. 6. Density of states of the fcc Al-Zn alloys as a function of energy (relative to the Fermi energy ε_F) at different alloy compositions. DOS peaks discussed in the text are marked with arrows.

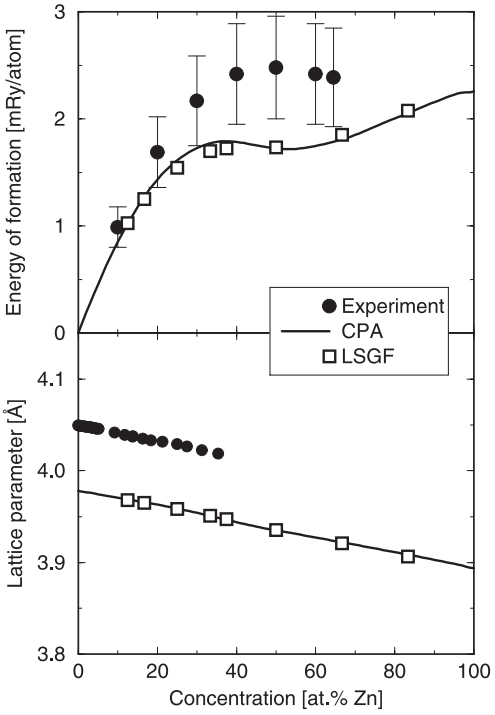

Fig. 7. Energy of formation (a) and lattice parameter (b) of random Al-Zn alloys as a function of concentration. Experimental data are taken from reference [17] (enthalpy of formation) and reference [67] (lattice parameter).

Thus, as has been pointed out above, the coexistence of several ETTs of different kind in a narrow concentration interval at around 45 at. % of Zn leads to a strong peculiarity (a minimum) in the DOS. According to equation (3) one can expect a superior stability of an alloy whose Fermi level falls into the DOS minimum. As a matter of fact, this conclusion is consistent with the Hume-Rothery criterion of alloy stability [1] which has been recently re-examined by Paxton *et al.* [6]. The behavior of the mixing energy in the Al-Zn system adheres to this criterion.

4.3 Influence of the ETT on the thermodynamic properties of Al-Zn alloys

The calculated energy of formation and the lattice parameters of disordered fcc Al-Zn alloys are shown in Figure 7. Attention must be called to the fact that we have taken into account the experimentally derived energy difference between the fcc and hexagonal structures for pure Zn, 2.26 mRy [19]. According to our results, no ordered or disordered alloys are stable at zero temperature, although their positive enthalpies of formation are rather small. This indicates that, due to their chemical proximity, Al and Zn have rather weak tendency to form intermetallic compounds or towards phase separation. In spite of the fact that the small enthalpies of formation in Al-Zn system are at the edge of accuracy of total energy calculations by the LMTO-ASA-CPA method, the numerical agreement of theoretical and experimental results is quite good. Our results are also in satisfactory agreement with recent full-potential calculations by Müller *et al.* [22] Calculated lattice parameters of fcc Al-Zn alloys are underestimated by about 2% compared to experiment, but their concentration dependence is well reproduced in our study.

We have also estimated the free energy of formation of disordered alloy, $F(c) = E(c) - TS$, taking into account only the configuration entropy in a mean field approximation, $S_{conf} = -k_B[c\ \ln(c) + (1-c)\ \ln(1-c)]$. Figure 8 shows that the free energy of Al-Zn alloys, which is positive at low temperatures, gradually becomes negative when the temperature increases. At approximately 400 K, the α_2 phase becomes stable at $\sim$ 53 at.% Zn concentration (experimentally, the temperature of this transition is 548 K [17]). At temperatures above 400 K, we find that two fcc phases, α_1 and α_2, are in equilibrium. Reduced temperature of monotectoid transformation can be explained by the fact that the enthalpy of formation obtained in our LMTO-CPA-ASA calculations is underestimated compared to the experimental data. Also, we

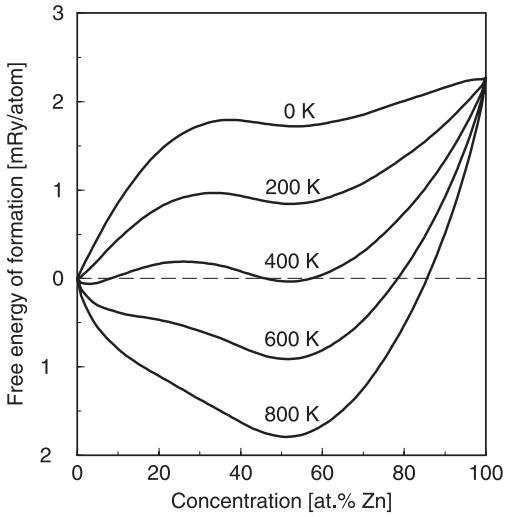

Fig. 8. Evolution of the free energy of random Al-Zn alloys with temperature. Only the mean-field configurational entropy term is included.

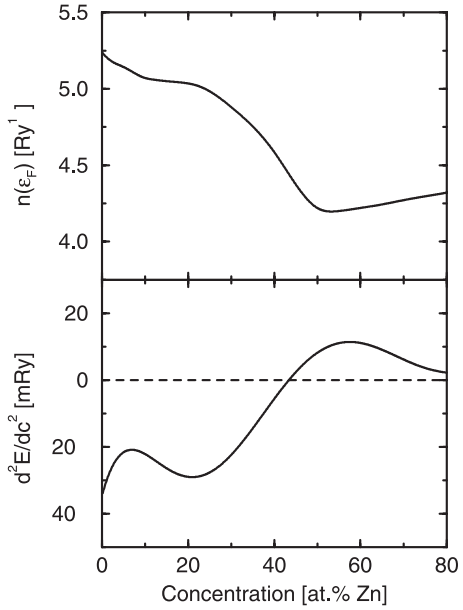

Fig. 9. (a) Density of states at the Fermi energy and (b) the second derivative of the mixing energy as a function of Zn concentration within the stability range of fcc Al-Zn alloys.

correctly predict the width of miscibility gap, however obtained concentrations of α_1 and α_2 phases deviate somewhat from corresponding values on the phase diagram. The main reason for this deviation consists of using the ASA for the total energy calculations. Our calculations predict that the miscibility gap closes up at 800 K, that is above the experimental data. It can be explained by the fact that we have calculated the free energies of completely random alloys, whereas it is known that real Al-Zn alloys exhibit a certain degree of short-range order [22,66]. Thus, the most important features of the Al-Zn phase diagram are reproduced in our study, and we conclude that mixing energies calculated in this work are suitable for a qualitative analysis of the physical phenomena that lead to the particular topology of this diagram.

In order to establish an influence of the ETT on the energy of mixing in fcc Al-Zn alloys, let us first point out that a simple consideration based on the chemical proximity and a small size mismatch between Al and Zn could lead one to an expectation that a model of regular solid solutions should describe the energetics in this system. According to this model the mixing energy $E_{mix} \sim c(1-c)$, *i.e.* it is symmetric relative to equiatomic composition, and $\mathrm{d}^2E_{mix}/\mathrm{d}c^2 = \text{const}$. However, due to ETT the $\mathrm{d}^2E_{mix}/\mathrm{d}c^2$ varies with concentration, equation (3). The strongest singularity of the DOS is due to the confluence of two ETT at ~ 45 at % of Zn. They occur when the Fermi level passes a DOS valley between peaks B and C at ~ 50 at % of Zn. Therefore, relative stability of random alloys as a function of concentration deviates from the model of regular solid solutions, and the mixing energy, as well as the miscibility gap on the Al-Zn phase diagram, become assymetric with respect to equiatomic composition. To justify this conclusion even further, we have plotted in Figure 9 the density of states at the Fermi energy (panel a) and the second derivative of the mixing energy (panel b) as a function of Zn concentration in fcc Al-Zn alloys. According to equation (3) these two curves must anticorrelate with each other as they indeed do (Fig. 9). Note, that small deviations can be explained by the fact that equation (3) considers only the band energy term, while in practice we have obtained the E_{mix} from the total energy calculations. It is noteworthy, that there is a concentration region in which the sign of the second derivative is positive, $50-55$ at.% Zn. The positive sign of the second derivative means that these alloys are metastable, *i.e.* some nucleation energy is necessary to initiate a process of alloy decomposition. The alloys beyond this concentration interval are absolutely unstable with respect to the spinodal decomposition.

5 Summary

The electronic structure, Fermi surface and thermodynamic properties of fcc Al-Zn alloys were calculated within the stability range of the fcc solid solutions $0-70$ at.% of Zn. Our calculations were based on the density functional theory and employ a basis set of the linear muffin-tin orbitals in the atomic sphere approximation. We considered random Al-Zn alloys using two different approaches within alloy theory, the coherent potential approximation and the locally self-consistent Green's function (LSGF) method. We use a modified screened impurity model, SIM, for estimating the electrostatic contribution to the one-electron potential of an atom in an alloy, and to the alloy total energy. For selected set of alloy concentration we show that parameters of this model can be chosen in such a way that the CPA ASA calculations reproduce the LSGF calculations with multipole corrections to the ASA included

by means of the ASA+M method. The CPA calculations were then performed for random Al-Zn alloys in the whole concentration interval.

We found 7 electronic topological transitions in Al-Zn alloys in the concentration interval 0−70 at.% of Zn. There are two ETT that occur at about 45 at.% Zn. Coexistence of two ETT of different types in the narrow concentration interval leads to the strong singularity in the alloy density of states at the Fermi level. Due to this a relative stability of random Al-Zn alloys as a function of concentration deviates from the model of regular solid solutions, and the mixing energy, as well as the miscibility gap on the Al-Zn phase diagram, become assymetric with respect to equiatomic composition.

The collaboration between Sweden and the former Soviet Union was supported by The Royal Swedish Academy of Sciences and the Swedish Foundation for International Cooperation in Research and Higher Education (STINT). I.A.A. and B.J. are grateful to the Swedish Research Council, Natural and Engineering Sciences, for financial support. The Swedish Foundation for Strategic Research and the Russian Foundation for basic Research are gratefully acknowledged for financial support. This work was partially financed by SKB AB, the Swedish Nuclear Fuel and Waste Management Company.

References

1. W. Hume-Rothery, J. Inst. Met. **35**, 295 (1926); W. Hume-Rothery, G.V. Raynor, *The Structure of Metals and Alloys* (Institute of Metals, London, 1954)
2. H. Jones, Proc. R. Soc. London A **144**, 225 (1934); H. Jones, J. Phys. Rad. **23**, 637 (1962)
3. T.B. Massalski, U. Mizutani, Prog. Mater. Sci. **22**, 151 (1978)
4. A.G. Khachaturyan, *Theory of Structural Transformations in Solids* (John Wiley & Sons, New York, 1983), p. 99
5. B.L. Gyorffy, G.M. Stocks, Phys. Rev. Lett. **50**, 374 (1983)
6. A.T. Paxton, M. Methfessel, D.G. Pettifor, Proc. R. Soc Lond. A **453**, 1493 (1997)
7. J.F. Clark, F.J. Pinski, D.D. Johnson, P.A. Sterne, J.B. Staunton, B. Ginatempo, Phys. Rev. Lett. **74**, 3225 (1995)
8. I.M. Lifshitz, Zh. Eksp. Teor. Fiz. **38**, 1569 (1960) [Sov. Phys. JETP **11**, 1130 (1960)]
9. S. Egorov, A.N. Fedorov, Zh. Eksp. Teor. Fiz. **85**, 1647 (1983) [Sov. Phys. JETP **58**, 959 (1983)]
10. A.A. Varlamov, V.S. Egorov, A.V. Pantsulaya, Adv. Phys. **38**, 1647 (1983)
11. V.G. Vaks, A.V. Trefilov, J. Phys. F **18**, 213 (1988)
12. M.I. Katsnelson, I.I. Naumov, A.V. Trefilov, Phase Transitions **49**, 143 (1994)
13. Ya. M. Blanter, M.I. Kaganov, A.V. Pantsulaya, A.A. Varlamov, Phys. Rep. **245**, 159 (1994)
14. I.A. Abrikosov, Yu. H. Vekilov, P.A. Korzhavyi, A.V. Ruban, L.E. Shilkrot, Solid State Commun. **83**, 867 (1992)
15. N.V. Skorodumova, S.I. Simak, I.A. Abrikosov, B. Johansson, Yu. Kh. Vekilov, Phys. Rev. B **57**, 14673 (1998); N.V. Skorodumova, I.A. Abrikosov, S.I. Simak, B. Johansson, Yu. Kh. Vekilov, Philos. Mag. B **78**, 565 (1998)
16. E.A. Smirnova, P.A. Korzhavyi, Yu. Kh. Vekilov, B. Johansson, I.A. Abrikosov, Phys. Rev. B **64**, 020101 (2001)
17. R. Hultgren, P. Desai, D.T. Hawkins, M. Gleiser, K.K. Kelley, *Selected Values of Thermodynamic Properties of Binary Alloys* (American Society for Metals, Metals Park, Ohio, 1973), p. 228
18. F.E. Witting, L. Schöffl, Z. Metallkd. **51**, 700 (1960)
19. S. an Mey, Z. Metallkd. **84**, 451 (1993)
20. J. Mainville, Y.S. Yang, K.R. Erder, M. Sutton, K.F. Ludwig Jr, G.B. Stephenson, Phys. Rev. Lett. **78**, 2787 (1997)
21. P. Zięba, Z. Metallkd. **90**, 669 (1999)
22. S. Müller, L.-W. Wang, A. Zunger, C. Wolverton, Phys. Rev. B **60**, 16448 (1999)
23. S. Müller, C. Wolverton, L.-W. Wang, A. Zunger, Acta Mater. **48**, 4007 (2000); Europhys. Lett. **55**, 33 (2001)
24. A.V. Ruban, H.L. Skriver, J. Nørskov, Phys. Rev. Lett. **80**, 1240 (1998)
25. H.L. Skriver, Phys. Rev. B **31**, 1909 (1985)
26. U. Häussermann, S.I. Simak, R. Ahuja, B. Johansson, S. Lidin, Angew. Chem. Int. Ed. **38**, 2017 (1999)
27. P.A. Korzhavyi, E.A. Smirnova, I.E. Eybelman, I.A. Abrikosov, A.V. Ruban, Yu. Kh. Vekilov, Phys. Solid State **39**, 515 (1997)
28. Recently, a treatment of ETT that includes effects of electron correlations has been given by M.I. Katsnelson, A.V. Trefilov, Phys. Rev. B **61**, 1643 (2000)
29. V. Heine, D. Weaire, Solid State Phys. **24**, 249 (1970)
30. M.I. Katsnelson, G.V. Peschanskih, A.V. Trefilov, Fiz. Tverd. Tela **32**, 470 (1990); V. Yu. Irkhin, M.I. Katsnelson, A.V. Trefilov, J. Magn. Magn. Mater. **117**, 210 (1992)
31. P. Hohenberg, W. Kohn, Phys. Rev. B **136**, 864 (1964)
32. W. Kohn, L.J. Sham, Phys. Rev. **140**, A1133 (1965)
33. J.P. Perdew, K. Burke, M. Ernzerhof, Phys. Rev. Lett. **77**, 3865 (1996)
34. O.K. Andersen, Phys. Rev. B **12**, 3060 (1975)
35. O. Gunnarsson, O. Jepsen, O.K. Andersen, Phys. Rev. B **27**, 7144 (1983)
36. H.L. Skriver, *The LMTO Method* (Springer-Verlag, Berlin, 1984)
37. O.K. Andersen, O. Jepsen, Phys. Rev. Lett. **53**, 2571 (1984)
38. O.K. Andersen, O. Jepsen, D. Glötzel, in *Highlights of Condensed-Matter Theory*, edited by F. Bassani, F. Fumi, M.P. Tosi (North Holland, New York, 1985)
39. O.K. Andersen, Z. Pawlowska, O. Jepsen, Phys. Rev. B **34**, 5253 (1986)
40. D.J. Chadi, M.L. Cohen, Phys. Rev. B **8**, 5747 (1973)
41. P. Soven, Phys. Rev. **156**, 809 (1967)
42. B.L. Györffy Phys. Rev. B **5**, 2382 (1972)
43. J.S. Faulkner, Prog. Mater. Sci. **27**, 1 (1982)
44. I.A. Abrikosov, H.L. Skriver, Phys. Rev. B **47**, 16532 (1993)
45. I.A. Abrikosov, A.M.N. Niklasson, S.I. Simak, B. Johansson, A.V. Ruban, H.L. Skriver, Phys. Rev. Lett. **76**, 4203 (1996)
46. I.A. Abrikosov, S.I. Simak, B. Johansson, A.V. Ruban, H.L. Skriver, Phys. Rev. B **56**, 9319 (1997)
47. G.M. Stocks, B.L. Györffy, E.S. Giuliano, R. Ruggeri, J. Phys. F **7**, 1859 (1977)
48. W.M. Temmerman, B.L. Györffy, G.M. Stocks, J. Phys. F **8**, 2461 (1978)
49. J.S. Faulkner, G.M. Stocks, Phys. Rev. B **21**, 3222 (1980)

50. E. Bruno, B. Ginatempo, E.S. Giuliano, A.V. Ruban, Yu. Kh. Vekilov, Phys. Rep. **249**, 355 (1994)
51. N.V. Skorodumova, S.I. Simak, E.A. Smirnova, Yu. Kh. Vekilov, Phys. Lett. A **208**, 157 (1995)
52. D.D. Johnson, M. Asta, Comput. Mater. Sci. **8**, 54 (1997)
53. I.A. Abrikosov, B. Johansson, Phys. Rev. B **57**, 14164 (1998); I.A. Abrikosov, A.V. Ruban, B. Johansson, H.L. Skriver, Comput. Mater. Sci. **10**, 302 (1998)
54. J.S. Faulkner, N.Y. Moghadam, Y. Wang, G.M. Stocks, Phys. Rev. B **57**, 7653 (1998); B. Ujfalussy, J.S. Faulkner, N.Y. Moghadam, G.M. Stocks, Y. Wang, Phys. Rev. B **61**, 12005 (2000)
55. D.M.C. Nicholson, G.M. Stocks, Y. Wang, W.A. Shelton, Z. Szotek, W.M. Temmerman, Phys. Rev. B **50**, 14686 (1994)
56. Y. Wang, G.M. Stocks, W.A. Shelton, D.M.C. Nicholson, Z. Szotek, W.M. Temmerman, Phys. Rev. Lett. **75**, 2867 (1995)
57. S.I. Simak, A.V. Ruban, I.A. Abrikosov, H.L. Skriver, B. Johansson, Phys. Rev. Lett. **81**, 188 (1998)
58. H.L. Skriver, N.M. Rosengaard, Phys. Rev. B **46**, 7157 (1992)
59. P.A. Korzhavyi, I.A. Abrikosov, B. Johansson, A. V. Ruban, H.L. Skriver, Phys. Rev. B **59**, 11693 (1999); P.A. Korzhavyi, A.V. Ruban, A.Y. Lozovoi, Yu. Kh. Vekilov, I.A. Abrikosov, B. Johansson, Phys. Rev. B **61**, 6003 (2000)
60. P.A. Korzhavyi, A.V. Ruban, S.I. Simak, Yu. Kh. Vekilov, Phys. Rev. B **49**, 14229 (1994)
61. P.A. Korzhavyi, A.V. Ruban, I.A. Abrikosov, H.L. Skriver, Phys. Rev. B **51**, 5773 (1995)
62. A.V. Ruban, I.A. Abrikosov, H.L. Skriver, Phys. Rev. B **51**, 12958 (1995)
63. D.D. Johnson, F.J. Pinski, Phys. Rev. B **48**, 11553 (1993)
64. A.V. Ruban, H.L. Skriver, Phys. Rev. B **66**, 024201 (2002); A.V. Ruban, S.I. Simak, P.A. Korzhavyi, H.L. Skriver, Phys. Rev. B **66**, 024202 (2002)
65. B.E.A. Gordon, W.E. Temmerman, B.L. Gyorffy, J. Phys. F **11**, 821 (1981)
66. E.T. Emirbekov, Fiz. Metall. i Metalloved. **68**, 1135 (1989), in Russian [Translated in: Physics of Metals and Metallography]
67. W.B. Pearson, *A Handbook of Lattice Spacing and Structure of Metals and Alloys* (Pergamon Press, London, 1967)